Supplement of Nat. Hazards Earth Syst. Sci., 22, 2381–2400, 2022
https://doi.org/10.5194/nhess-22-2381-2022-supplement

Natural Hazards and Earth System Sciences
Open Access
EGU

Supplement of

Developing a framework for the assessment of current and future flood risk in Venice, Italy

Julius Schlumberger et al.

Correspondence to: Julius Schlumberger (j.schlumberger@posteo.de)

Contents

List of Figures

List of Tables

1 Analysis of damage claim data-set for unexpected meteorological event of 12 November 2019

This chapter provides a more detailed insight into the available damage claim data of residents and entities issued with regards to the consequences of the 12 November 2019 storm surge event. First, some general insights are provided. In addition, a more detailed analysis of the immediate response claim data as well as the full damage claim data-set is provided to investigate possible relations between the amount of damage claims and the modelled water levels inside the old-town of Venice. Information of the calibrated and validated hydrodynamic model as presented in the main paper were used for this analysis.

1.1 Background on available damage claim data set

As a response to the unexpected extreme meteorological event of 12 November 2019, financial support to affected parties was provided according to art. 25 (2) of decree n.1/2018[1]: first economic measures of immediate support to the economic and social fabric could be claimed with regards to letter c) of the decree; residents were able to submit bills and damage estimates that would be compensated up to 5,000 EUR. The same applied for entities (companies, NGO's,...) up to a maximum of 20,000 EUR. For structural damages exceeding the other budgets, a separate form according to letter e) of the decree was provided to cover for the restoration of damaged public and private structures and infrastructures, as well as the damage suffered by economic and productive activities, cultural and landscape assets and the building heritage. An overview of damages that were eligible to be accounted for is given in the section 1.5 at the end of this chapter.

Residents and entities were entitled to apply for damage compensation in one or both categories depending on the experienced damages. In total 7,644 claims were issued inside the study area with a total volume of about 56,2 million Euro, see table S1. While immediate response claim data could be directly linked to physical assets[2], this was not possible for the damage cost data in the categories 'combined' or 'letter e) only' for privacy reasons. For the latter two, data were only available on a city district level.

Table S1: Number and total volume [EUR million] of damage claims per stakeholder group in million EUR. Aggregated over study area Provided by the office of Delegate Commissioner of Venice

	letter c) only		combination		letter e) only	
	claims	volume	claims	volume	claims	volume
residents	1,382	3.85	367	2.96	630	6.24
non residential	2,345	23.14	369	13.60	142	6.43
total	3,728	26.99	736	16.55	772	12.67

[1]accessed here: `https://www.gazzettaufficiale.it/eli/id/2018/1/22/18G00011/sg`
[2]accessed here: `https://www.commissariodelegato.venezia.it/`

1.2 Immediate Response Claim analysis

1.2.1 Allocating damage claims to structures

A set of 33,096 addresses[3] was used to link the immediate response claims to the structures inside the study area, as visualized in the workflow of figure S1. 32,956 addresses could be allocated to structures. The remaining 140 addresses were mostly related to open areas without buildings and therefore neglected in the further process. Using the set of available addresses, it was possible to link 95 % of the reported entity claims and 97% of the residential immediate response claims to buildings inside the study area, see table S2. The total 3,728 immediate response claims could be linked to 2,778 buildings.

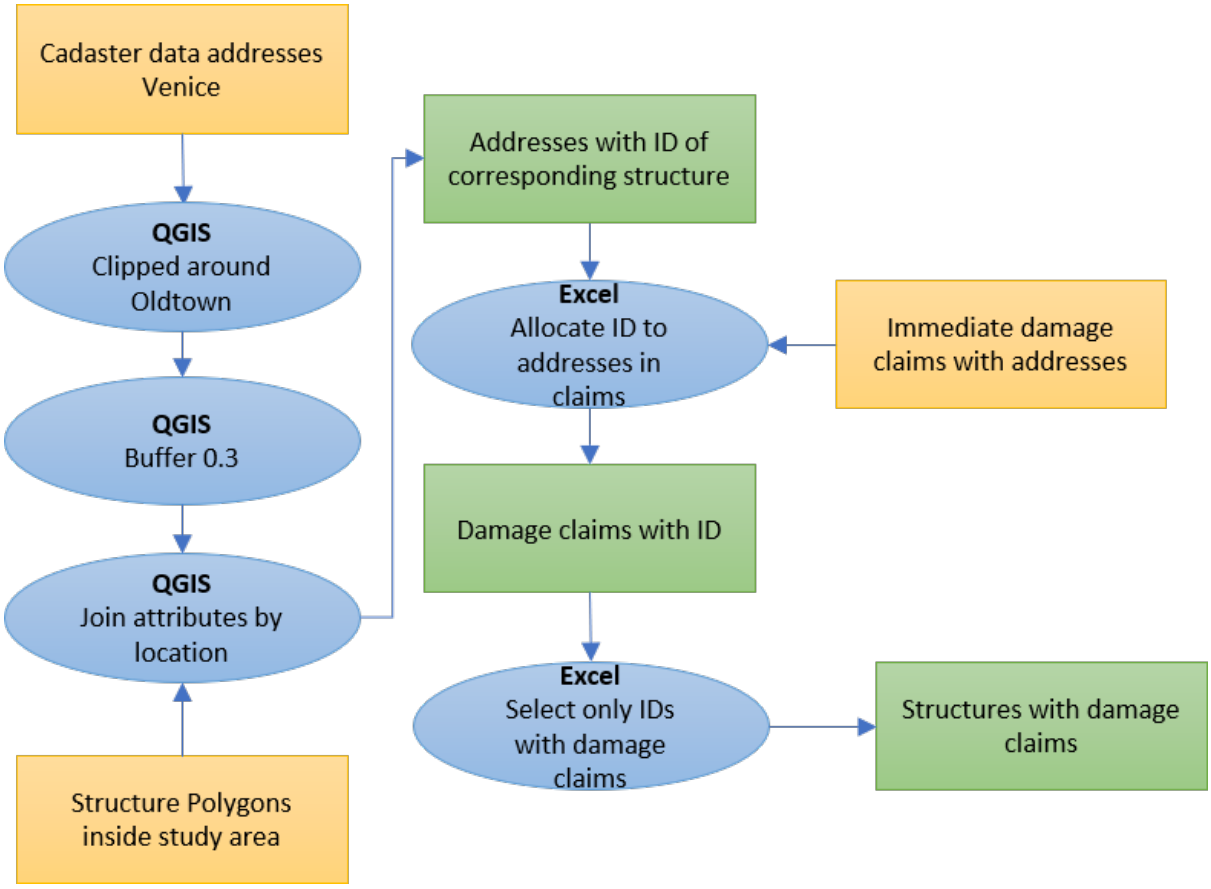

Figure S1: Workflow to allocate immediate response claims to structures inside study area

Table S2: Share of immediate response claims allocated to addresses inside Venice

	reported claims [EUR]	allocated claims [EUR]	efficiency
residential claims	3.85E+06	3.73E+06	0.97
entity claims	2.31E+07	2.20E+07	0.95

[3]accessed here: `https://portale.comune.venezia.it/node/117/12181978`

1.2.2 Analysis of depth-damage correlation

Two different correlations between flood depth and immediate response damage claims were considered. Initially, every individual claim was plotted against the average flooding depth at the building. Secondly, damage claims were aggregated for neighborhoods, here represented by the 14,460 buildings. In Venice, couple of addresses were often linked to the same building. It was tested whether the absolute damage claims per structure showed some correlation with the average flooding depth. Figure S2 shows some exemplary results, meanwhile correlation values for the considered cases is compiled in table S3. Accordingly, it can be concluded, that those immediate response data seem insufficient to derive any reliable relation with the simulated water levels. Further processing steps, like normalizing the aggregated neighborhood claims by means of the area of the structure (assuming constant reconstruction cost per m^2) did also not improve the results.

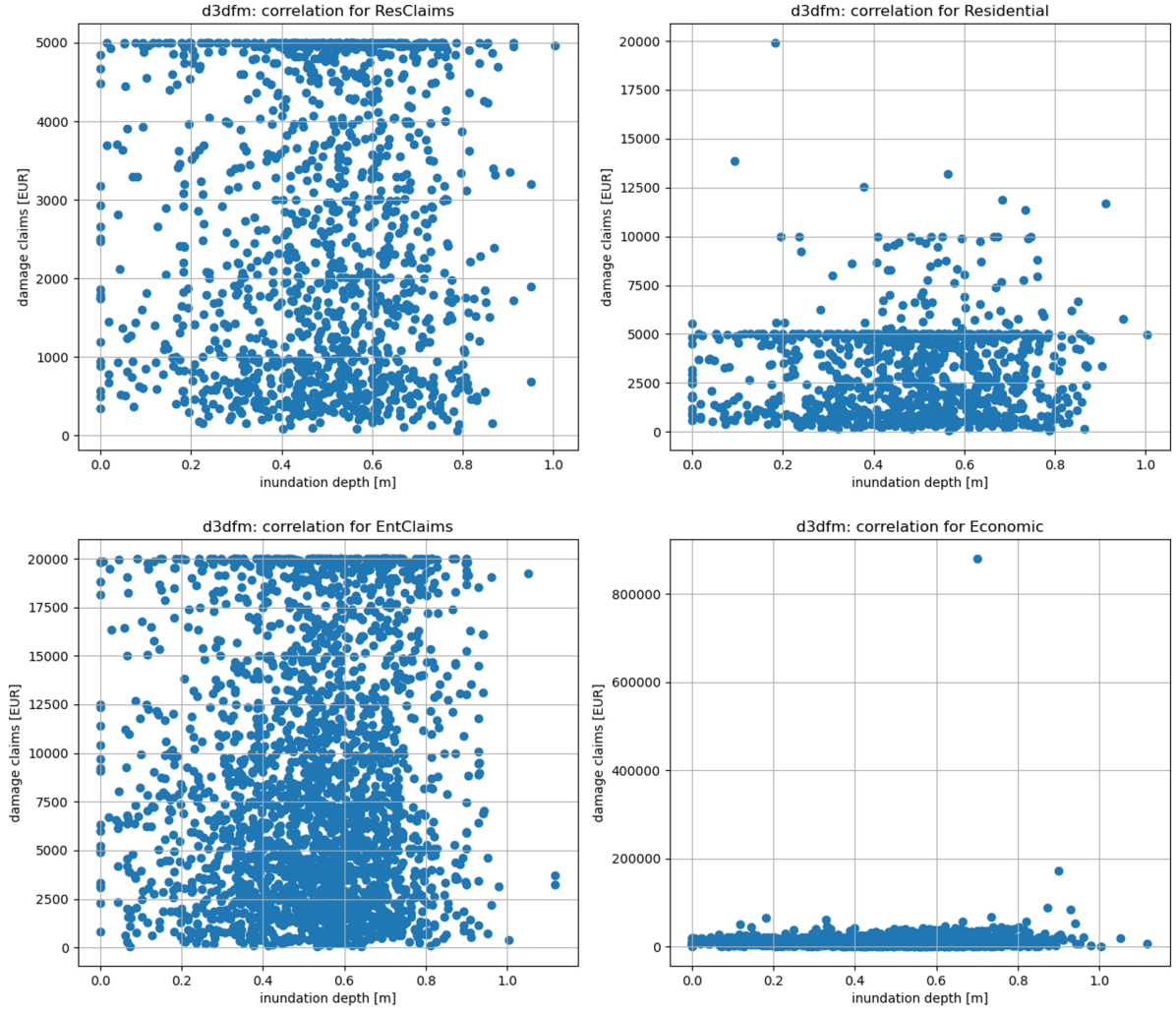

Figure S2: Scatter plots for visualization of correlation between water depth and immediate damage claims. Left: individual claims. Right: claims aggregated if referenced to same building (neighborhood).

Table S3: Pearson correlation for water depth and immediate response claims. Comparison for different approaches of hazard modelling

	bathtub	d3dfm
Neighborhood Residential	0.060	0.076
Neighborhood Entities	0.045	0.060
Neighborhood combined	0.063	0.078
Individual Residential	0.000	0.000
Individual Entities	0.037	0.047

1.3 Analysis of full set of damage claims

To analyse possible depth-damage claim relations of the full data set, it was necessary to use all information averaged and aggregated on a district level, because this was the level of detail of the damage claim data set. To analyse depth-damage claim relations on the meso-scale, the aggregated damage claims on district levels were compared against a mean flood depth in the respective district. The flood depth was hereby derived as the average depth of flooding of all structures in the district. Additionally, the number of claims compared to the number of structures inside the district were compared against the average flood depth. Three claim sets were used: total damage claims by residents, entities and the combination of both. Results are shown in figure S3.

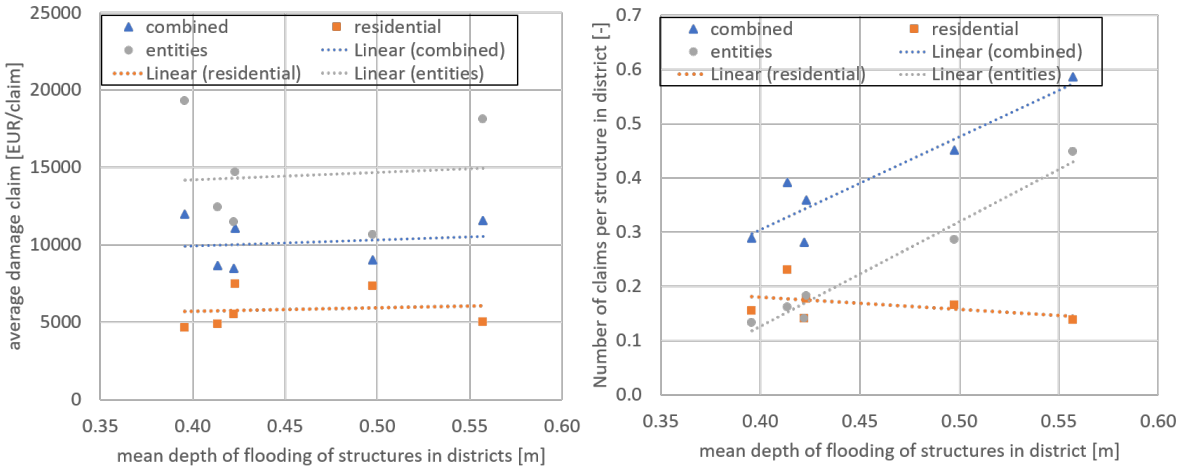

Figure S3: Left: Relation between average depth of flooding and the average damage claims. Right: Relation between number of claims and average depth of flooding

These results open up room for interesting interpretations. It can be seen that for entities, a stronger positive trend between both number of claims and average claim volume and the average water depth is detectable. Moreover, the analysis suggests that there is even a negative correlation between average flood depths and number of residential damage claims. Meanwhile one possible interpretation could be that residents in lower-lying districts are more aware of the potential flood damages as they experienced flooding personally more frequently in the past. Therefore they might be more risk averse or better

prepared. This might also reflect in almost constant values of average damage claims for different water levels. However, this hypothesis on the claims ratio is contradicted by the strong trend for the entities. A possible explanation could be that entities are less risk aware (which is a hypothesis presented here without proof or indications). Alternatively, general differences between the constitution of structure use and protection measures of the different districts could play a role. This means that in one district the share of residential used ground floors might be much higher than in others. As a matter of fact, the district with the maximum average water level is San Marco, a district which is highly touristic and used for commercial purposes. However, as limited information on the real distribution of entities and residential use of ground floors is not available in the required detail and completeness, above hypotheses cannot be confirmed or rejected.

1.4 Possibility to derive empirical model

Using the maximum inundation depth as the driving hazard characteristic is commonly applied but can only be used if no other flood characteristics like flow velocity, wave action or contamination cause major damages [1]. Given overall low flow velocities and limited wave action [2], damage models depending mainly on depth-damage relations are particularly applicable in a context like Venice, where most direct damage is expected to occur due to hydrostatic forces.

On the other hand empirical models that have been developed for damages of a very specific flood event are rather limited in their transferability [3]–[5]; they significantly depend on the quality, type and amount of damage data available for deriving damage relations; meanwhile extensive expert field work and reporting of damages is helpful to derive a full picture of effective damages [1], damage information are often more scarce or derived from damage compensation claims which might be incomplete; even if damage data are available from authorities or insurance companies, it has been questioned whether the registered damage claims fully represent the effective damages [6]. Often, reimbursement is made available only for a specific set of properties or purpose. Also, limited public budgets result in strict requirements for reimbursement, which also reduce the expectation of residents and therefore their willingness to submit claims. Another identified limitation is related to the recovery behavior based on the available budgets and attitude. Some will have the capacity to fully replace any affected property, others might just select a path of recovery to restore its functionality.

In this specific case couple of limitations were discovered that might suggest that the available damage claim data set is not appropriate to develop empirical depth-damage relations for Venice. Firstly, the low spatial resolution introduces significant uncertainty as the systems of flood protection along with exposure are reported to vary significantly. In addition the low spatial resolution of total damage claim volumes requires to use averaged flood depth information as well. As Venice is a generally low lying city without significant altimetric variation, this leads to a very narrow flood depth range for which the model could be used. Furthermore, any derivation of a depth-damage relation on district level would only be based on 6 data points and can therefore provide only a limited degree of confidence for the extrapolation of the fitted relation.

1.5 Eligible damage claims acccording to art. 25 (2) of decree n.1/201

Residents could claim compensation for the following damages:

- Structural elements
- Internal and external finishes
- Internal and external windows and doors
- Heating, water and sewage systems (including sanitary)
- Electrical system
- Elevator, stair lift
- Pertinence connected to the main building
- Pertinence distinct from the structural unit in which the dwelling is located but functional to the use of the same
- Exterior area and grounds
- Any adjustments required by law
- Technical services (design, supervision works, etc.), including charges (social security)
- Kitchen furniture
- Bedroom furniture

Entities could claim compensation for the following damages:

- Machinery and equipment
- Stocks of raw materials, semi-finished and finished products
- Refreshment room furnishings and related household appliances
- Damage to structural and non-structural parts:
  - Structural elements
  - Internal and external finishes
  - Internal and external windows and doors
  - Heating systems, water and sewerage (including sanitary facilities)
  - Electrical and alarm systems
  - Intercom systems, LAN data network
  - Elevator, stair lift
  - Pertinence
  - Area and external fund
  - Any adjustments required by law
  - Technical services (design, construction management, etc.), including charges (social security).
- Rental of property or other temporary solution, reconstruction in the same site or relocalization in another site of the municipal:

2 Development of hydrodynamic model

2.1 Reasoning for choice of hydrodynamic model

For this study, a 2D hydrodynamic model based on Delft3D Flexible Mesh Suite 2021.03 is used. The software provides a flexible unstructured grid framework allowing for coupling of unstructured grids consisting of triangles, quadrangles, pentagons and hexagons [7]. Furthermore, Delft3D Flexible Mesh Suite 2021.03 allows for the coupling of different modules:

- D-Flow FM is a multi-dimensional (1D, 2D and 3D) hydrodynamic simulation scheme
- D-Real Time Control which allows the consideration of dynamic hydraulic structures
- D-Waves (SWAN) to account for wave propagation and wave-induced set up

- D-Morphology for a simulation of sediment transport

Applying D3DFM instead of re-using and refining existing models of the Venetian lagoon was preferred due to two reasons: firstly, the flexible character of the grid simplifies the grid generation significantly [8]. Secondly, even though this study only considers a 2D-implementation of D-Flow and a basic closure function for the MOSE barrier, future studies can easily build on the developed model and set up integrated models using above mentioned modules for a better physical representation of the system, for example:

- Coupling of 1D-2D flow: Given information about the sewage system, coupling of respective flows can be easily integrated
- Coupling with D-Real Time control allows for the proper consideration of the MOSE barrier closure and opening process.
- Coupling with D-Waves could deal with the commonly used simplification of the surge event that generally neglects the influence of waves.
- Coupling with D-Morphology could account for advanced and more realistic changes in the tidal behaviour and flood propagation for sea level rise scenarios in medium or long-term future.

D-Flow FM uses the shallow water equations, which are a simplification of of the Reynolds-averaged Navier-Stokes equations (RANS). The mass and momentum conservation equations are implemented the following way:

$$\frac{\delta h}{\delta t} + \nabla * (hu) = 0 \tag{1}$$

$$\frac{\delta (hu)}{\delta t} + \nabla * (huu) = -gh\zeta + \nabla * (h\nu(\nabla u + \nabla u^T)) + \frac{\tau_b + \tau_w}{\rho} \tag{2}$$

where $\nabla = (\frac{\delta}{\delta x}, \frac{\delta}{\delta x})^T$, ζ is the water level, h the water depth, u the velocity vector, ν the viscosity, g the gravitational acceleration, ρ the water mass density, τ_b the bottom friction using the Chezy coefficient, and τ_w the wind friction.

2.2 Conversion of altimetry data

Altimetry data were derived from various sources with varying reference datum as shown in Tab.2 of the main paper. Conversion of the altimetry to the ZMPS datum were performed by adding or subtracting the absolute difference between the respective datum and ZMPS as conceptualised in Fig. S4. Accordingly, the bathymetry information of the Venetian lagoon and the canals within the old-town (both available in IGM42, where 0m IGM42 corresponds to + 0.23 m ZMP) were corrected by subtracting 0.23cm from the original IGM42-referenced altimetry data. The surface of the old-town of Venice (also provided in IGM42) was corrected by adding 0.23 cm given that the surface was generally located above the respective MSL. Altimetry information of the Adriatic shelf were provided with reference to the LAT datum which was assumed in this work to approximately correspond to -0.4m ZMPS. Consequently, bathymetry of the Adriatic shelf was corrected by adding +0.4 m.

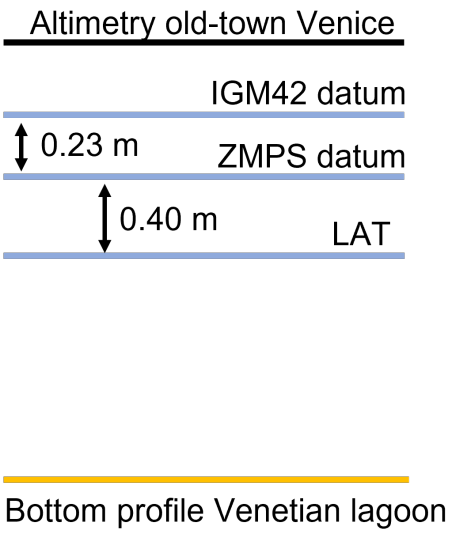

Figure S4: Schematisation of reference datum for input data

2.3 Creation of the model grid

The choice of modelling framework had to satisfy both, the complexity of the model domain and the required available modelling time. Even though Delft3D-FM is capable of running models with many millions of elements for extended time periods, the required computational time increases significantly with increasing complexity of the model. Water level time-series from the parent model simulation was extracted at 168 locations inside and around the old-town of Venice for calibration purposes as well as for inputs in the nested sub-models, see figure S5. These parent model outputs where then used to run 7 separate, nested models.

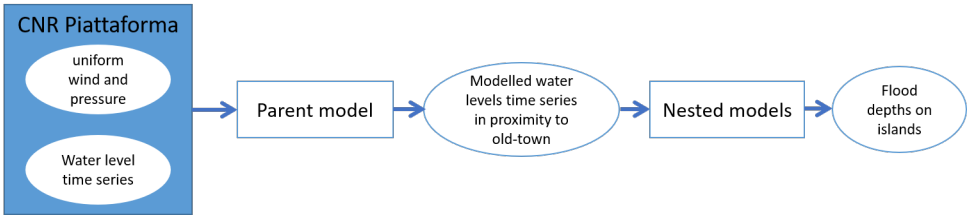

Figure S5: Framework of applied flood modeling approach

The computational grid of the coastal model was generated using the buit-in software provided by D-Flow using information on the extent of the lagoon and shape of the islands of the old-town of Venice [9][10]. The workflow for the grid generation is outlined in figure S6.

The process required frequent transfer of shape files into D-Flow grid inputs and vice versa. This conversion was done using Quickplot 2.60. In addition to the grid creation and merging activities, it was regularly checked that the used grids satisfy the requirements for the modelling, namely sufficient orthogonality and smoothness. Both requirements were maintained by using built-in function in RGFGRID.

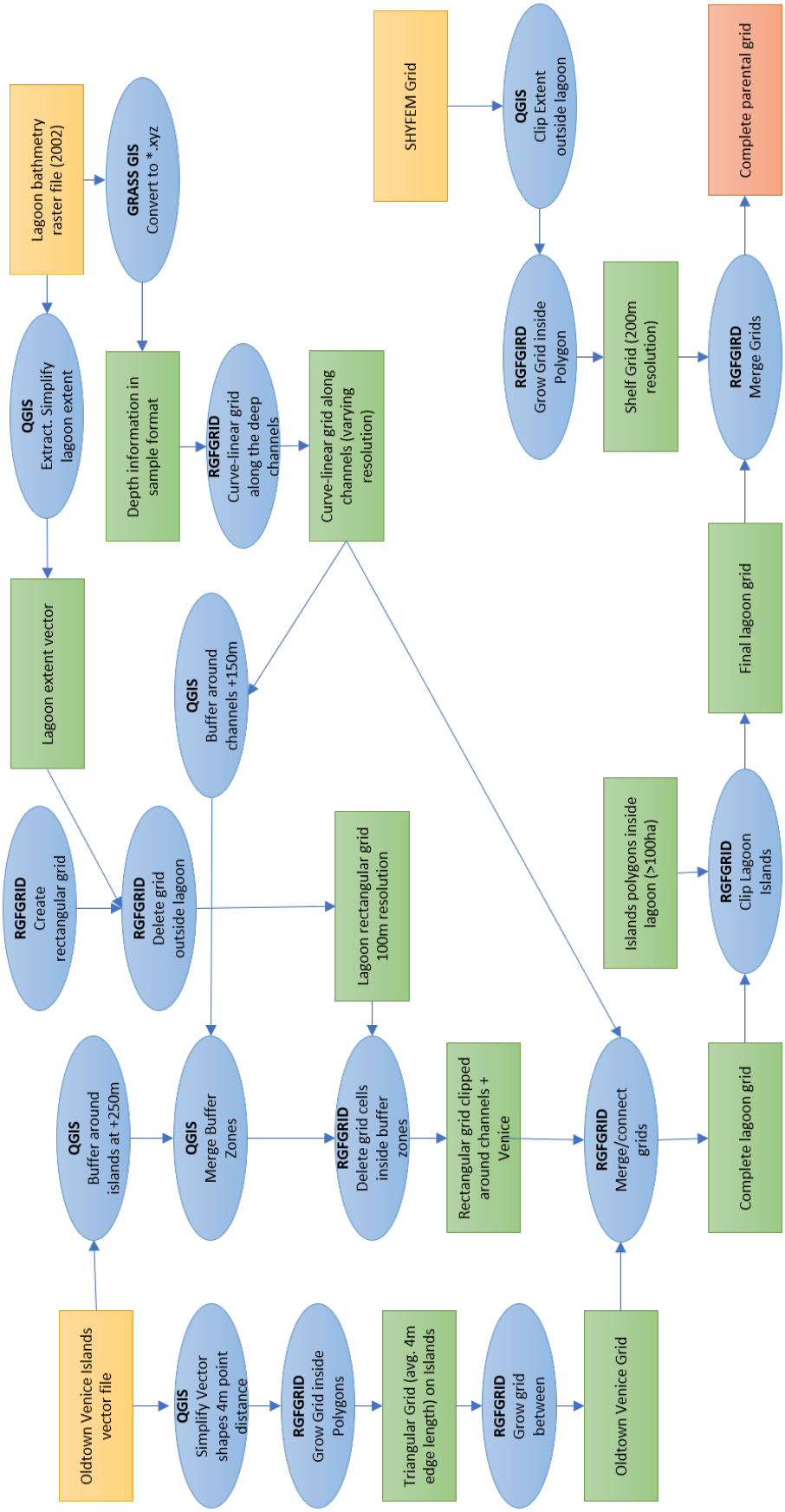

Figure S6: Workflow for the creation of the parent grid. Input files are highlighted in yellow, intermediate products in blue and the final product in red.

The final grid contained 2.73 million elements with an average resolution inside the lagoon of 100, at the shelf up to 200m and inside the area of the old-town of Venice between 2.6m at the islands and 15m in the canals. In the final parent grid, all grid elements that fell inside the buildings were clipped to avoid additional complex altimetry configurations.

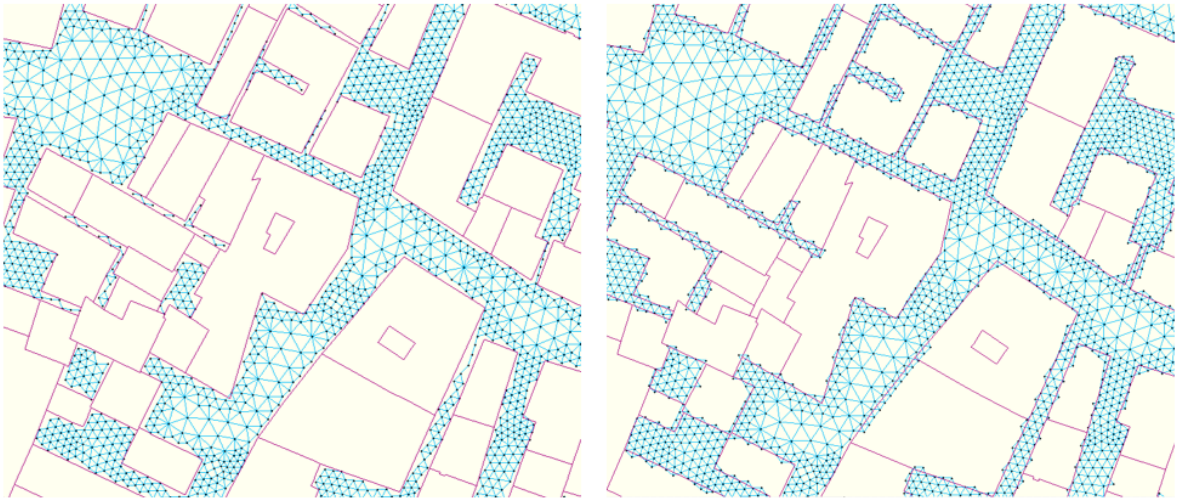

Figure S7: Example of grid continuity for different clipping polygons. Left: clipped grid using the original polygons of the structures. Many grid elements in narrow areas between buildings are reduced to lines (without flow). Right: clipped grid using the original polygons of the structures buffered by $-1m$. Most narrow streets are now interconnected by the grid elements.

For the nested sub-grids, a grid refinement around the structures in the old-town of Venice was done to improve the resolution of the narrow streets. Within a buffer of 4m around the structures, the grid was refined to about 1.3m on average. Again, the grid elements that fall inside the polygons of the structures were clipped; the structure perimeter was buffered by $-1m$ to account for the concept of the grid generation software used by D-Flow deleting grids inside polygons: every node that falls inside a polygon will be deleted and therefore the entire element. Applying the buffer of $-1m$ to the polygons and then use these polygons to clip grid elements inside the structures was found iteratively the best way to make sure that narrow streets were represented by a set of connected grid elements, as visualized in figure S7. Based on visual analysis, the benefit of a higher interconnection of narrow streets seemed significantly better than the effect of overestimation of the width of streets by a few grid elements.

2.4 Background on the closing process of the MOSE barrier

The decision on when to start closing the barrier depends on forecasts of precipitation, wind velocity and direction, inflow and expected return period of the expected event [11]. These estimates can be attributed to certain operational classes. Based on the operational class, the maximum water level at Punta della Salute at which the barrier starts closing can be determined, see table S4 for further details. The water level with a return period

of 10 years corresponding to the threshold between the two main operational classes is defined as the water level of 1.50 m+ZMPS at Punta della Salute [12]. For all scenarios, the flood event of 12 November 2019 would have lead to a class 2 operation. Thus, closure would have started as soon as water level would exceed 0.65m+ZMPS at Punta della Salute.

Table S4: Operation classes to determine the water level at which MOSE barrier starts closing. RP means Return period. Copied from [12].

Class	Sub-class	Closure level [m]
Class 1: $RP < 10yrs$, $u_{10} < 15m/s$	1A: rainfall: $< 1mm/h$, inflow $< 150m3/h$	1.00
	1B: rainfall: $> 1mm/h$, inflow $> 150m3/h$	0.90
Class 1: $RP < 10yrs$, $u_{10} > 15m/s$	1AV: rainfall: $< 1mm/h$, inflow $< 150m3/h$	0.80
	1BV: rainfall: $> 1mm/h$, inflow $> 150m3/h$	0.75
Class 2: $RP > 10yrs$	-	0.65

3 INSYDE model background & set-up

3.1 INSYDE parameters

The INSYDE model uses a set of 23 parameters to describe the flood event and exposed building. They either directly or indirectly influence the exposure extent or damage costs, see figure S8. Meanwhile some default values could be used from the original set up, other values had to be adjusted to better represent the typical residential building in Venice. Below table gives a summary of the used parameters.

Damage components			Event features							Building characteristics														
			External water depth (h_e)	Internal water depth (h)	Flow velocity (v)	Sediment load (s)	Duration (d)	Water quality (q)	Internal area (IA)	Basement area (BA)	External perimeter (EP)	Internal perimeter (IP)	Basement perimeter (BP)	Number of floors (NF)	Interfloor height (IH)	Basement height (BH)	Ground floor level (GL)	Basement level (BL)	Building type (BT)	Building structure (BS)	Finishing level (FL)	Level of maintenance (LM)	Year of construction (Y)	Heat. system distribution (PD)	Heat. system type (PT)
Clean-up	C1 – Pumping								x	x							x	x	x						
	C2 – Waste disposal			x		x		x	x	x						x		x	x						
	C3 – Cleaning			x				x	x	x		x			x	x		x	x						
	C4 – Dehumidification			x			x	x	x	x					x	x		x	x						
Removal	R1 – Screed			x			x		x						x			x		x					
	R2 – Pavement			x			x		x						x			x		x					
	R3 – Skirting			x			x					x			x			x							
	R4 – Partition walls			x			x					x			x			x		x					
	R5 – Plasterboard			x					x			x			x			x		x					
	R6 – External plaster		x				x	x			x							x			x				
	R7 – Internal plaster			x			x	x				x	x			x		x			x				
	R8 – Doors			x			x		x	x					x			x							
	R9 – Windows			x			x		x	x					x			x							
	R10 – Boiler			x					x	x					x			x							x
Non-structural	N1 – Partition replacements			x			x		x			x			x			x	x						
	N2 – Screed replacement			x			x				x				x			x		x					
	N3 – Plasterboard replacement			x					x		x				x			x		x					
Structural	S1 – Soil consolidation		x		x				x					x	x			x	x						
	S2 – Local repair		x		x	x					x							x	x						
	S3 – Pillar repair		x		x	x					x							x	x						
Finishing	F1 – External plaster replacement	x		x			x	x			x							x		x					
	F2 – Internal plaster replacement			x			x	x				x	x			x		x		x					
	F3 – External painting	x									x				x			x		x					
	F4 – Internal painting			x								x	x		x	x		x		x					
	F5 – Pavement replacement			x			x					x			x			x		x					
	F6 – Skirting replacement			x			x						x		x			x		x					
Windows and doors	W1 – Door replacements			x		x		x		x	x				x			x		x					
	W2 – Window replacements			x		x		x		x					x			x		x					
Building systems	P1 – Boiler replacement			x					x	x					x			x		x			x		
	P2 – Radiator painting			x					x						x			x							x
	P3 – Underfl. heating replacement			x			x		x						x			x		x					x
	P4 – Electrical system replacement			x					x						x			x		x					
	P5 – Plumbing system replacement			x				x	x						x			x		x					

Figure S8: Damage components and sub-components considered in INSYDE, and relationships with event features and building characteristics parameters. Copied from [4]

3.2 Assumptions and elaboration on available data

Several sources were used to obtain information on the exposure characteristics of the buildings. While some default values could be used from the original set up, other values

had to be adjusted to better represent the typical buildings in Venice. Table S5 gives a summary of the used parameters.

Table S5: Parameters to describe the exposed building types in the study area. BEA: 'building with economic activity on ground floor'.

	explanation	used default values	
		residential	BEA
FA	Footprint area $[m^2]$	cadastral data	
IA	Internal area $[m]$	$0.9 * FA$	
BA	Basement area $[m^2]$	0	
EP	External perimeter $[m]$	cadastral data	
IP	Internal perimeter $[m]$	2.5 * EP	1.5 * EP
IH	Interstorey height $[m]$	$3.5m$	
BH	Basement height $[m]$	0	
BP	Basement perimeter $[m]$	0	
GL	Groundfloor level $[m]$	0.1 m	0.0 m
NF	Number of floors	1	
BT	Building type	4	5
BS	Building structure	Census data	
PD	Plant distribution	1- Centralized	
PT	Heating system type	1- Radiator	
FL	Finishing Level	1- medium	
YY	Year of construction	Census data	
LM	Level of maintenance	Census data	
additional			
EP_{eff}	effective external perimeter	Cadastral data	
SH	surface elevation of building	City of Venice [10]	
CH	Cultural heritage status	Cultural Heritage office Venice	

Apart from the inundation depth which was calculated using the hazard models all other parameters were used as constants, see table S6. Given the highly dynamic character of the flood event defined by a rapid increase and decrease of maximum water level, the flood duration was assumed much lower than in the original set up of INSYDE. Given that presence of salt has been reported to cause additional deterioration at buildings in Venice [13][14], presence of pollutants was considered as an additional damage source.

Table S6: Parameters to describe the flood characteristics

	explanation	used value
he	water depth $[m]$	D3DFM result
v	velocity $[m/s]$	$0.3\frac{m}{s}$
s	sediment concentration [-]	0.05
d	flood duration [h]	2
q	presence of pollutants	yes

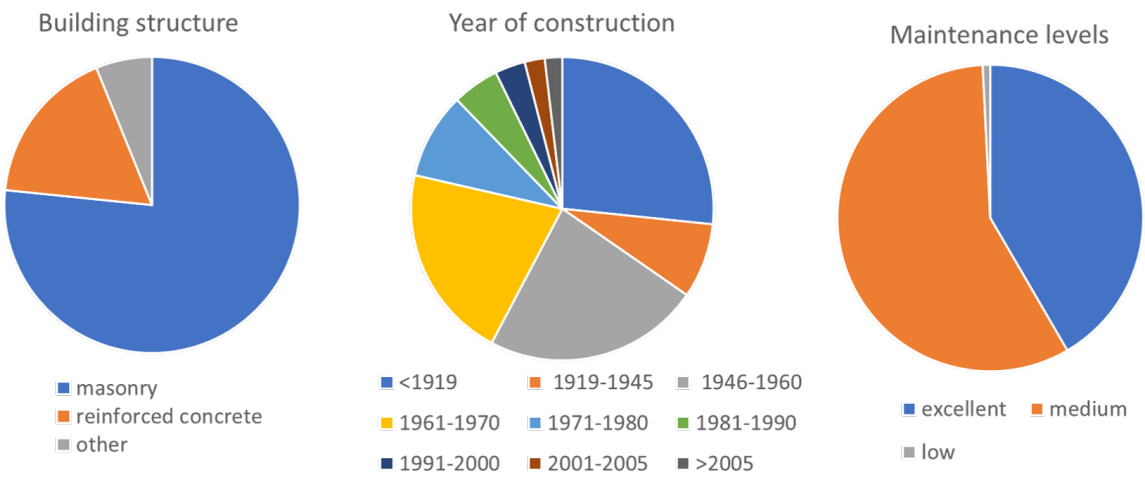

Figure S9: Summary of main exposure characteristics

Most recent census data information were available from ISTAT. These census block aggregate the main characteristics of the buildings within the census block. Below figures show the spatial distribution of some of the characteristics. The relevant parameters for INSYDE consider the level of maintenance, which was either excellent, good or fair, the year of construction the building structure which was majorly either reinforced concrete or masonry, see figure S9. An additional analysis was conducted to investigate the spatial distribution, see figure S10, figure S11, and figure S12. Because of the spatial variation it was decided to allocate the relevant exposure characteristics per census block using the most frequently present realization. For census blocks without any information for a given category, the most frequent characteristic as derived from figure S9 was used.

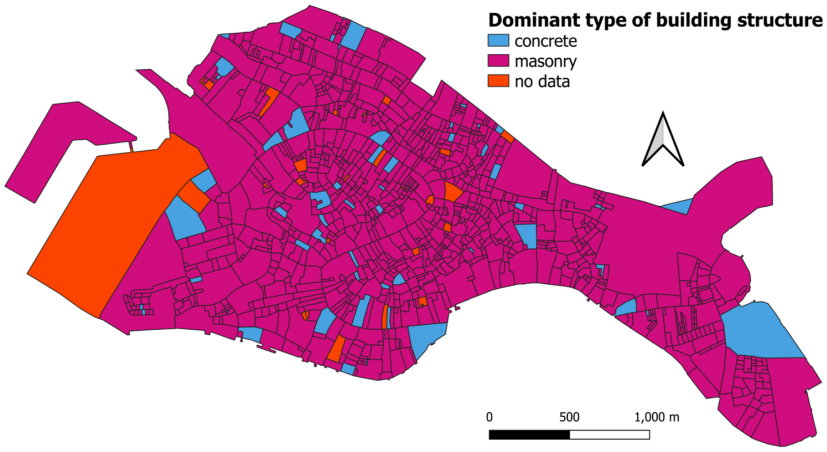

Figure S10: Spatial variation of the share of masonry structure on census block resolution.

For the construction year, which is distinguished in periods, the mean year was used. For buildings with a construction year earlier than 1919, 1919 was chosen, meanwhile for buildings constructed later than 2005, the year 2010 was used. In addition, indication of the number of parties living within one structure could be derived. Analysis of the census block data suggests that not more than two parties live in 57 % of the residential structures in the study area.

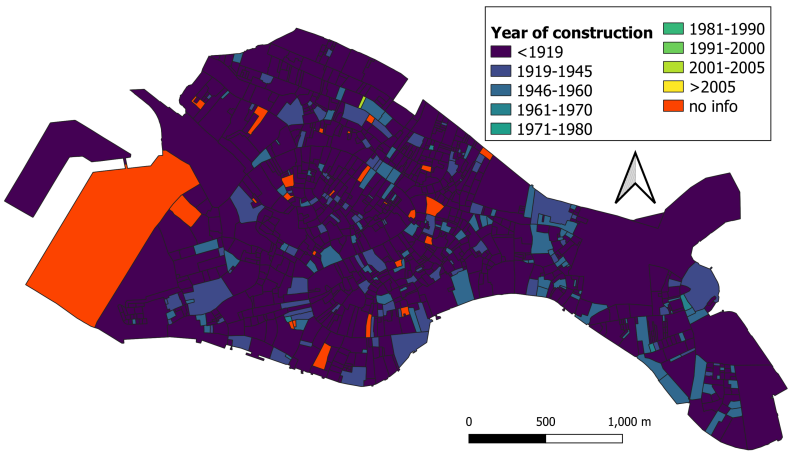

Figure S11: Spatial variation of the most frequent construction year on census block resolution

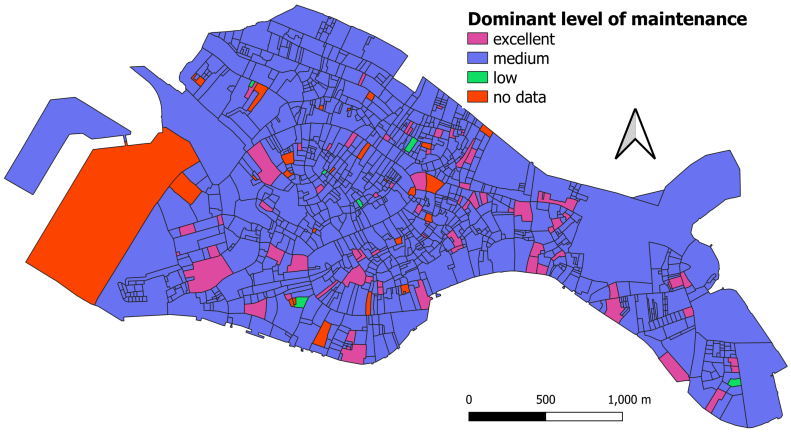

Figure S12: Spatial variation level of maintenance on census block resolution

3.3 Method to calculate the effective external perimeter

Other than EP which provides the exact perimeter of the building and is used to derive the internal perimeter, EP_{eff} describes the effective external wall perimeter exposed to flood. EP_{eff} accounts for the fact that most buildings in Venice are attached to each other resulting in just one or two walls exposed to water.

The effective external perimeter of each structure $EP_{eff,i}$ was computed using QGIS by substracting the total length of shared perimeter with neighbored buildings from the original perimeter length. The following querry code for a virtual layer[4] was used to identify the neighbors of each structure and length of shared boundary:

```
SELECT u11.*, GROUP_CONCAT(u12.id || ', len:' ||
round(st_length(st_intersection(u11.geometry, u12.geometry)), 4), "; ")
AS "neighbor_info"
FROM "structures" AS u11, "structures" AS u12
```

[4]accessed here: https://gis.stackexchange.com/questions/360760/calculating-length-of-common-boundary-lines-of-two-polygon-in-qgis

```
WHERE st_intersects(u11.geometry, u12.geometry) AND u11.id <> u12.id
GROUP BY u11.id
ORDER BY u11.id ASC
```

It has to be noted that for some buildings, the above code did overestimate the length of shared borders at some buildings. This was observed mainly at buildings with complex structure resulting in intermediate gaps between two buildings that shared a common boundary. To correct for that, the following code was used to set the respective attributes, assuming a minimum perimeter length of structures of 8 m:

```
if( "sharedBorder" is null, "Perimeter" , if("Perimeter" -
"sharedBorder"<2,"Perimeter" /4,"Perimeter" - "sharedBorder"))
```

4 Additional elaboration on hydrodynamic modelling results

4.1 Visualization of calibration results for tidal gauge stations

In the main paper, calibration results for the tidal gauge station Punta della Salute are shown. Figure S13 compiles the calibration results for the remaining tidal gauges considered in this study.

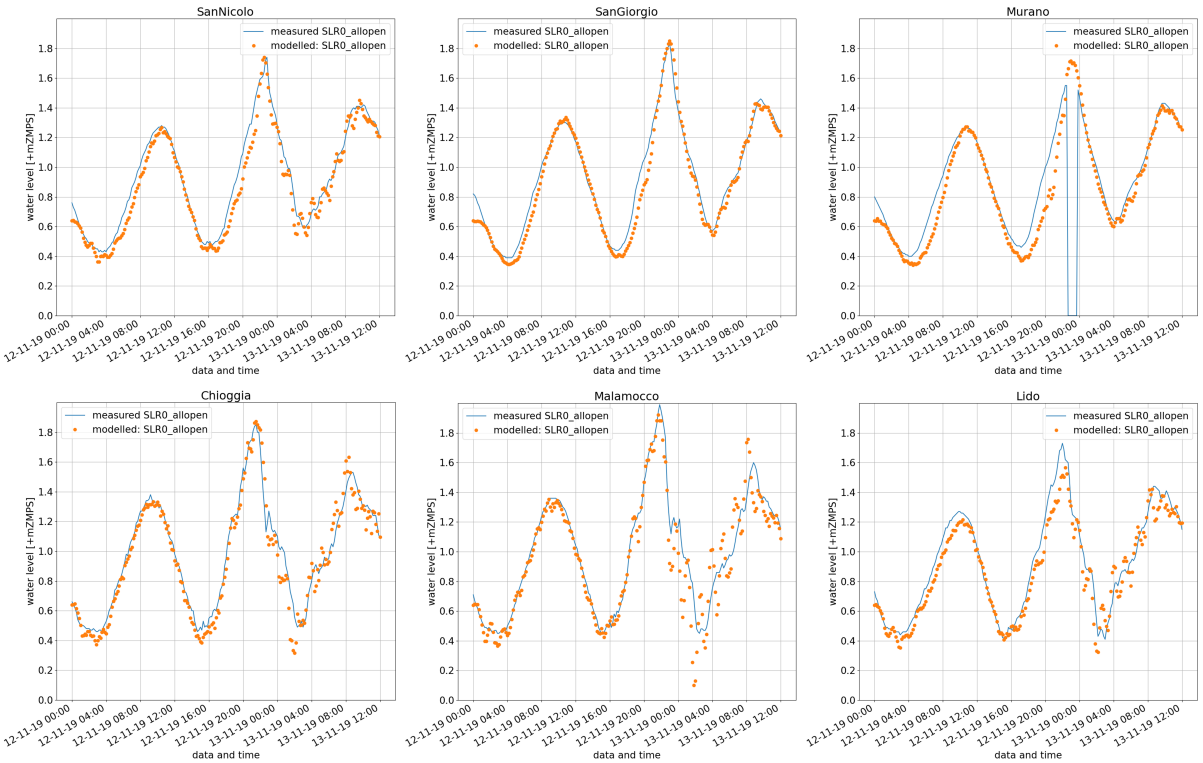

Figure S13: Modelled water levels of 12 Nov'19 storm surge compared against measured data at the other considered tidal gauges.

4.2 Effect of wind drag coefficient

For the 12 November 2019 storm event, the peak at Punta della Salute is underestimated (while it is slightly overestimated at the tidal gauges San Giorgio in Alga and San Nicolo, see figure S13). In general performance of the hydrodynamic parent model is good as outlined in the main paper. At the same time some deviations from the measured water levels were detectable which might be attributed to too high wind drag coefficients as suggested in figure S14. Time series of the wind suggest that a persistent strong north-easterly wind blows over the lagoon pushing the water away from the old-town until 21:40. Then, the wind turns into a very strong south-westerly wind, pushing water again towards the city. The model accounting for the effect of the wind first underestimates and then overestimates the water level, implying that the wind effect is too strong. This hypothesis is supported by a model run without taking the wind into account as visualized in figure S14: the simulated water level follows the measured time series closely until the strong south-westerly winds start to pick up. A similar observation was made for the validation run where the overestimation of the peak water level again coincides with a period of the strongest winds around 15:00 at 29 Oct 2018 pushing water towards the city of Venice. As in this study only a limited number of events were considered, it would be interesting to see how the model performs using more surge events to make some calibration adjustments of the wind drag and bottom friction if needed.

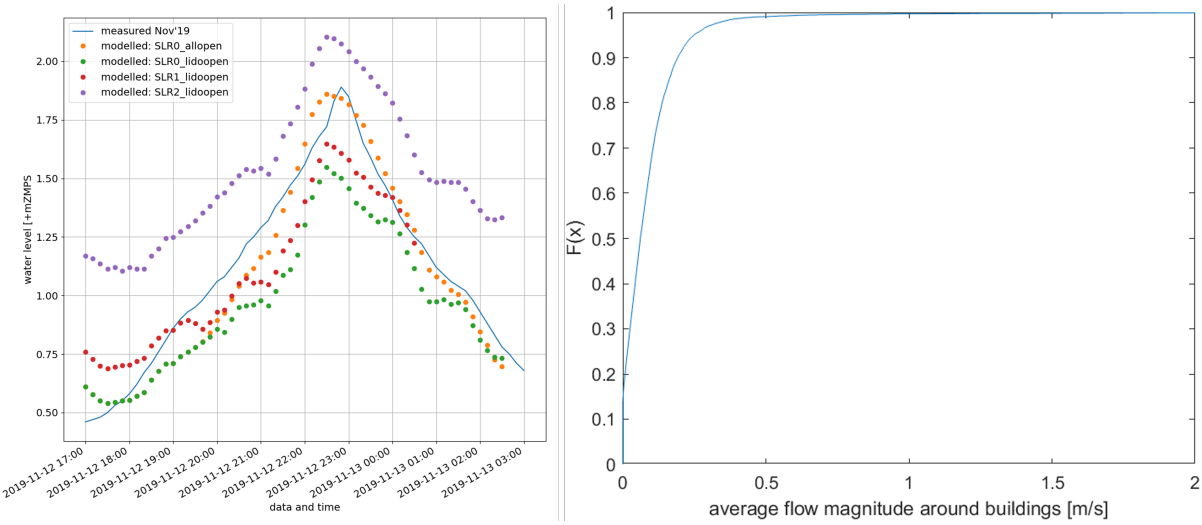

Figure S14: Left: Influence of meteorological forcing on the tidal signal at Punta della Salute for 12 Nov'19. Right: Share of buildings exposed to certain maximum flow velocities for SLR0-allopen.

4.3 Flow velocities inside old-town

It has been mentioned in the main paper that the maximum flow velocities inside the old-town are very low. Figure S14 justifies this claim. It can be seen that flow velocity is lower for 95% of the buildings. For some buildings, particularly along the main canals or in proximity of local instabilities, flow velocities were partly higher given that flow velocities. However, since the set up of the INSYDE model only accounts for the flow

velocity as an additional source of damage as of a flow velocity of 1.5 m/s, no additional damage due to flow velocities were expected in the study area.

5 Incorporating cultural heritage into the existing flood risk assessment scheme

5.1 Background on damage modelling of cultural heritage

The general flood characteristics causing damage to cultural heritage have been investigated [15]. Given the flood characteristics and regularity of flood event, the following mechanisms were selected as the dominant ones in the context of Venice:

- hydrostatic horizontal forces that can cause failure or deformation straight during the load condition
- Saturation of materials with water that can cause lasting deformation or damage to timber frames, walls and plaster.
- contamination of materials by chemical properties.

Meanwhile the first mechanism is relatively simple to understand and monitor given that the damages due to failure or deformation occur during the load conditions, other processes are less obvious or take much longer times before effects are visible. For example the effect of salt water on colours of paintings or frescoes which are highly hydrophil or sensitive to pH variation as well as to masonry walls is often not directly visible. In case of masonry wall it was found that particularly a repeated exposure to saltwater causes damage - linking such damages to one flood event is therefore very difficult [13]. Consequently, the estimation of total damage to cultural heritage is more complex than in the typical damage assessment. Even more, since cost and feasibility of various conservation actions (protection, restoration, reconstruction) are difficult questions that regularly take years to be answered. This is not only true for movable cultural heritage as happened in Florence [16], but also for immovable cultural heritage sites like St. Mark's basilica in Venice: the flood of 1966 significantly damaged masonry and mosaics, while restoration works started in 2003 [14].

Built cultural heritage encompasses historic buildings such as museums, churches, libraries and archives, as well as historic structures such as bridges, water infrastructure, historic landscapes and archaeological sites [17]. These sites typically have a high economic, scientific, religious, and historic values alongside social and cultural values (the last two often termed intangible values) RohitJigyasuManasMurthyGiovanniBoccardiChristopherMarrionDianeDouglasJosephKingGeo.2013. If damaged by floods, built heritage require special conservation, restoration and reconstruction efforts which can significantly affect the total tangible damages [18]. Thus, assessment of flood risk to cultural heritage should integrate factors that go beyond the physical properties of the exposed elements in order to quantify expected cultural losses.

Despite the fact that Italy is the first country to consider the flood risk to cultural heritage in the 1990s, a more robust quantification of damage to cultural sites is still an

ongoing research question because of different reasons [19]; most cultural heritage sites are unique and site-specific and thus often limited in their transferability [20]. Another challenge related to the quantification of intangible damages relates to the subjective character of the loss perception. While tangible damage can be easily translated into the metrics that are equal/similar for all people (monetary value), intangible damages lack such a universal metric. Moreover, the perception of cultural value or loss may differ within society as well as between different cultures [21]. A commonly used method is therefore risk rating matrices which link expected outcomes derived from qualitative or quantitative criteria to the likelihood of a certain event [21].

In literature various approaches and tools have been developed to assess risks to cultural heritage; while some focus on the hazard mapping [22],[23],[24], others apply simple approaches to identify the risk of exposed cultural heritage sites based on their rough classification [20], [18] or develop cultural value indicators and integrate them in risk frameworks [17]. Many scholars highlight that their work is rather a starting point for the assessment of historic buildings at risk.

An example is given for Florence, where the cultural risk is determined as low, medium or high on some basic assumptions of the difference between different building types with regards to the presence of cellar and whether the cultural value stems from the building and immovable contents or the movable ones [18]. Even if such an approach can give some first indication of cultural exposure, it is questionable whether the gained additional knowledge is useful given the generic and broad assumptions.

A more detailed approach has been developed for cultural heritage along the rivers in Portugal by the development of a heritage flood risk index [20].Based on the cultural heritage status (world heritage, national monument,...), a value was assigned to certain buildings. Based on six vulnerability classes ranging from 'rock art' to 'buildings with flood-susceptible contents of significant value', synthetic depth damage relations (here as depth-flood damage impact index relations) were developed under the assumption that the damage increases linearly up to maximum at a water level threshold. The product of the flood damage impact index and the cultural value of the building was used to derive the flood risk. The authors highlight that this method is again rather useful as a starting point for the assessment of potential buildings at risk. Due to its focus on providing a framework for a country-wide risk assessment, the available categories and resolution seemed insufficient for this work.

Dassanayake et al. [17] provides a framework that allows for a sophisticated and detailed consideration of a cultural heritage site. The approach is based on the assumption that cultural loss occurs to the same degree as the physical damage. The authors determine the level of cultural value of buildings characterised by their historical and social significance using a set of three proxies (age, spatial scale of importance, number of visiting tourists). Different categories of the level of physical damage are identified using depth-damage curves of a concrete structure and other findings from literature, see figure S15. Both, level of physical damage and level of cultural value are expressed on a scale from one to five. Averaging the value of physical damage and value of cultural value give a cultural risk indicator on a scale between one and five that could be used in a flood risk approach.

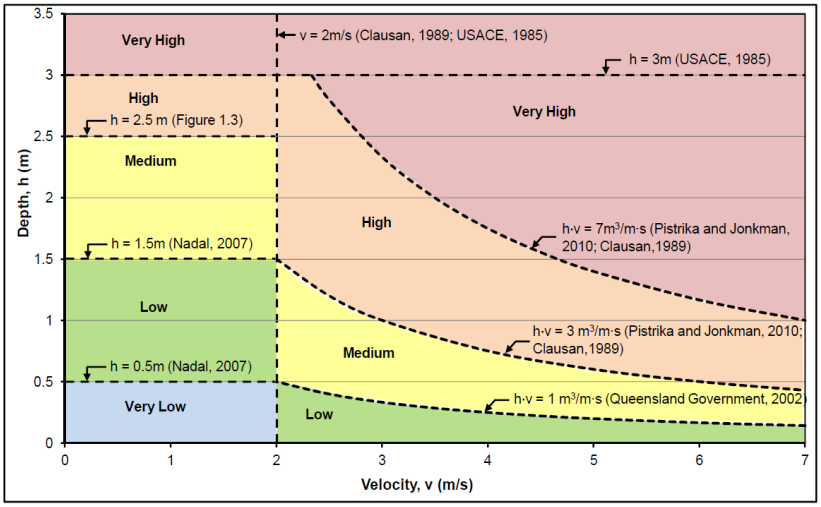

Figure S15: Applied damage categories in [17] and where they were derived from.

This approach seams appealing due to several reasons: while many studies in the field of cultural risk assessment use very broad categories to differentiate between cultural heritage sites, Dassanayake et al. [17] use a more sophisticated parametric approach to derive cultural values. This allows for a higher and more accurate differentiation of the cultural heritage sites in a study area, even if more than one site of the same building type is present; for example, in Venice there is a significant number of churches and chapels. Being able to differentiate their cultural value as much as possible provides a better insight in the real distribution of cultural flood risk given that most cultural indicators are just relative metrics. Secondly, the approach to derive a final cultural loss estimate taking into account the damage curve of an existing building shows the potential of this approach: if a unique depth-damage function for a cultural heritage site can be developed, a much better estimate of the respective cultural loss can be made.

Based on above considerations, an adjusted novel framework based on Dassanayake et al. [17] is proposed here: instead of using the cultural value assessment scheme used in the original study, it was decided to use a more sophisticated, robust and transparent framework developed for diverse historic buildings listed on the National Register of Historic Places (United States) [25]. Instead of the used damage categories derived from depth-damage curves of residential buildings, it was attempted to create a depth- damage relation for cultural heritage sites in Venice.

5.2 Proposed cultural heritage assessment scheme

5.2.1 Damage Categories

In the study, the INSYDE model was chosen to estimate flood damages to historic buildings in Venice. The big advantage of INSYDE compared to other models is that it is transparent and uses an explicit definition of exposure of different elements of a building that can be affected by flood events. As such, adding new building elements which are characteristic for cultural heritage along with information about their vertical distribution, damage ratio estimates, and reconstruction cost it can develop a damage curve that

represents a cultural heritage building type (e.g. 'church') or even of one very specific building (e.g. 'San Marco basilica') better than a generic depth damage curve. This approach also allows for application in other contexts such as when (new) local flood protection measures are installed or if the vertical distribution of value is adjusted.

In order to derive damage categories, a slightly different approach is used compared to [17]. INSYDE provides a relation between water depth and damages. In Dassanayake et al [17] the damage categories are based on the relative damage. No information on the typical reconstruction costs for churches is available, required to normalize experienced damages to identify the degree of physical damage. Consequently, for each building the highest reconstruction costs following a flood event should be investigated (probably after flood event in 1966) and used for the normalization. The damage categories could then be determined as shown in figure S16. The damage category boundaries are chosen such that cultural loss is estimated high if the reconstruction costs of the considered flood event are in the range of the maximum historic reconstruction costs, while the additional cultural loss for flood events corresponds to less than half of the flood reconstruction effort is defined as low. This approach seems reasonable to account for the fact, that no absolute maximum reconstruction value can be provided for a cultural heritage site. Using the maximum reconstruction value of the past allows to consider new damages always relative to the past events, meaning that new, flood events that exceed previous reconstruction costs always indicate significant new cultural damages.

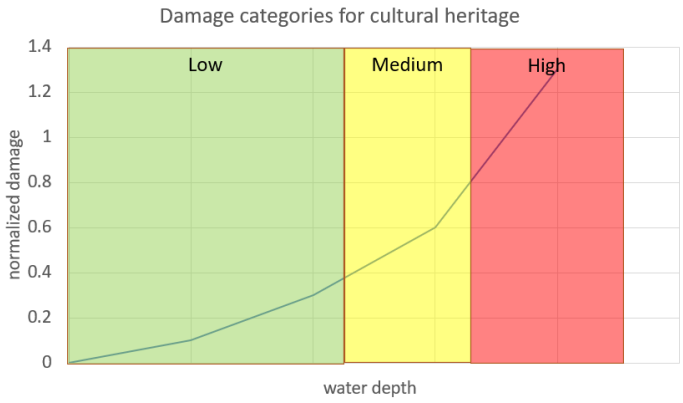

Figure S16: Adapted Damage categories for cultural heritage in Venice

5.2.2 Cultural Value Assessment

The applied framework for the assessment of cultural value should be adjusted from the framework developed for the historic buildings in the US [25]. The authors identified historical significance and use potential, characterised by nine sub-parameters in total, and allocated values as well as weighting factors in workshops with different experts. However, given the different national context, not all of the parameters could easily be transferred to the Venetian context or might be weighted equally.

The transferred list of the parameters and their definition as used in this study is given in table S7 at the end of this chapter. For two parameters, no corresponding parameter in the Italian context were found. Two other parameters were slightly adjusted. The final overview set of parameters and weights reads as shown in figure S17.

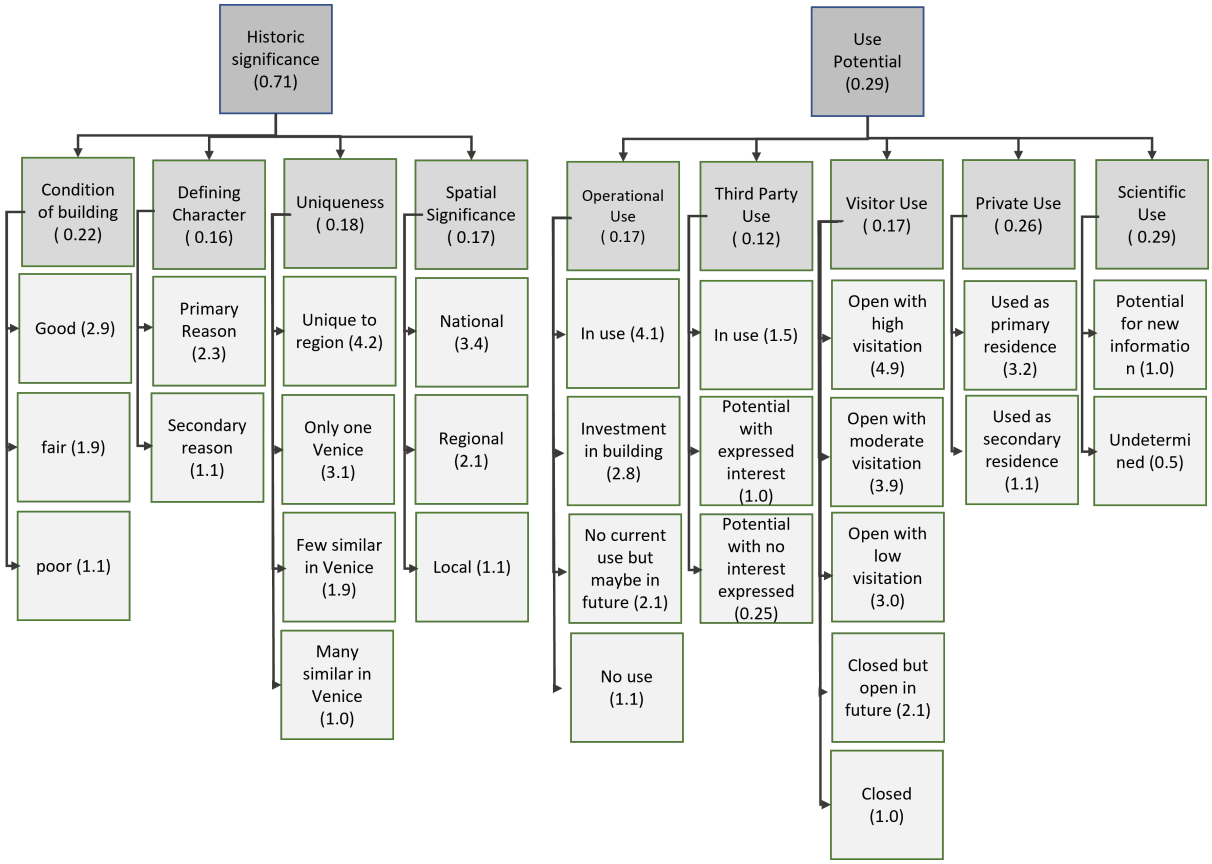

Figure S17: Set of parameters, values and weights applied to the Oldtown of Venice. Adjusted from [25]

For the list of selected cultural heritage sites, expert judgment supported by the experience and knowledge of the ecclesiastical cultural heritage office in Venice should be used. The cultural value CV of buildings according to [25] is computed the following way:

$$CV = w_{HS} * \sum_{i=1}^{4} w_i * h_i * w_{UP} * \sum_{j=1}^{5} w_j * u_j \tag{3}$$

where h_i, u_j are the respective values for the parameters describing the historic significance and use potential and w_i, w_j are the corresponding importance weights. The cultural values are normalized using the maximum possible value.

The cultural loss is then calculated by as the normalized product of the cultural value and the damage category based on the present normalized reconstruction costs, nrc:

$$CL = \frac{1}{3} * CV * DC \text{ , where } DC = \begin{cases} 1 & nrc \leq 0.4 \\ 2 & 0.4 \leq nrc \leq 0.8 \\ 3 & 0.8 \leq nrc \end{cases} \tag{4}$$

5.3 Elaboration on the parameters of cultural value

In table S7 parameters used in the present study are explained which are built using a framework by Fatoric and Seekamp [25]. Based on the descriptions the strong refer-

ence to the considered study area is very clear: four out of the nine parameters have a strong reference to a program or policy inside the study areas. Of these, it was decided to skip two parameters ('Association to fundamental purpose' and 'Eligibility of listing in National Registry of Historic Places'). Their weights are evenly distributed over the remaining parameters. 'Spatial significance' which refers to the US National Register of Historic Places can be directly replaced by its pendant in Italy. The 'interpretative use' is replaced by 'private use' which determines whether a historic buildings is used as a primary or secondary private residence/home.

Table S7: Sub-Parameters and their definition used in the present study

Parameter	Description
Condition of the historic building	Condition categories are assigned to structures/buildings as good, fair, or poor. Condition scores reflect the physical condition of the historic building.
Defining character	Refers to historic building's chronologic development in the historic city. Building is the primary (historical) reason that resulted in the development (or resettlement) of the historic city, or is part of the secondary development (or resettlement) of the historic city that occurred because of the original construction.
Uniqueness	Considers the original (historical) function of the historic building
Spatial significance	Considers geographical scale of a building's historic context that is listed in the register (i.e. national, regional or local)
Operational use	Using expert knowledge and technical judgment, the parameter evaluates whether or not the historic building is used for city operations, or has potential for it in the future. It also evaluates possible investment in the historic building for city operations in order to reduce the operational use of non-historic (non-contributing) building.
Third party use	This parameter assesses a use of the historic building by the third party though lease agreements and concessions.
Visitor use	The parameter explores current and future active uses of the building
Private use	This parameter assesses whether or not the historic building's is used as a private home (primary or secondary residence).
Scientific use	This parameter evaluates whether or not the historic building has a potential to yield new scientific information and value.

References

[1] A. K. Pistrika and S. N. Jonkman, "Damage to residential buildings due to flooding of new orleans after hurricane katrina," *Natural Hazards*, vol. 54, no. 2, pp. 413–434, 2010, ISSN: 1573-0840. DOI: 10.1007/s11069-009-9476-y.

[2] G. Umgiesser, "The impact of operating the mobile barriers in venice (mose) under climate change," *Journal for Nature Conservation*, vol. 54, p. 125 783, 2020, ISSN: 1617-1381. DOI: 10.1016/j.jnc.2019.125783.

[3] M. Amadio, J. Mysiak, L. Carrera, and E. Koks, "Improving flood damage assessment models in italy," *Natural Hazards*, vol. 82, no. 3, pp. 2075–2088, 2016, ISSN: 1573-0840. DOI: 10.1007/s11069-016-2286-0.

[4] F. Dottori, R. Figueiredo, M. L. V. Martina, D. Molinari, and A. R. Scorzini, "Insyde: A synthetic, probabilistic flood damage model based on explicit cost analysis," *Natural Hazards and Earth System Sciences*, vol. 16, no. 12, pp. 2577–2591, 2016, ISSN: 1561-8633. DOI: 10.5194/nhess-16-2577-2016. [Online]. Available: https://nhess.copernicus.org/articles/16/2577/2016/nhess-16-2577-2016.html.

[5] B. Merz and A. H. Thieken, "Flood risk curves and uncertainty bounds," *Natural Hazards*, vol. 51, no. 3, pp. 437–458, 2009, ISSN: 1573-0840. DOI: 10.1007/s11069-009-9452-6. [Online]. Available: https://www.researchgate.net/publication/227056811_Flood_risk_curves_and_uncertainty_bounds.

[6] D. Molinari, A. R. Scorzini, C. Arrighi, F. Carisi, F. Castelli, A. Domeneghetti, A. Gallazzi, M. Galliani, F. Grelot, P. Kellermann, H. Kreibich, G. S. Mohor, M. Mosimann, S. Natho, C. Richert, K. Schroeter, A. H. Thieken, A. P. Zischg, and F. Ballio, "Are flood damage models converging to "reality"? lessons learnt from a blind test," *Natural Hazards and Earth System Sciences*, vol. 20, no. 11, pp. 2997–3017, 2020, ISSN: 1561-8633. DOI: 10.5194/nhess-20-2997-2020. [Online]. Available: https://nhess.copernicus.org/articles/20/2997/2020/nhess-20-2997-2020-discussion.html.

[7] Deltares, "D-flow flexible mesh user manual,"

[8] R. C. Martyr-Koller, H. Kernkamp, A. van Dam, M. van der Wegen, L. V. Lucas, N. Knowles, B. Jaffe, and T. A. Fregoso, "Application of an unstructured 3d finite volume numerical model to flows and salinity dynamics in the san francisco bay-delta," *Estuarine, Coastal and Shelf Science*, vol. 192, pp. 86–107, 2017, ISSN: 0272-7714. DOI: 10.1016/j.ecss.2017.04.024. [Online]. Available: http://www.sciencedirect.com/science/article/pii/S0272771416307120.

[9] A. Sarretta, S. Pillon, E. Molinaroli, S. Guerzoni, and G. Fontolan, "Sediment budget in the lagoon of venice, italy: Continental shelf research, 30(8), 934-949," *Continental Shelf Research*, vol. 30, no. 8, pp. 934–949, 2010, ISSN: 0278-4343. DOI: 10.1016/J.CSR.2009.07.002.

[10] Learn_ArcGIS, *Map venice in 2d and 3d*, 9/2/2020. [Online]. Available: https://learn.arcgis.com/en/projects/map-venice-in-2d-and-3d/ (visited on).

[11] L. Zampato, M. Bajo, P. Canestrelli, and G. Umgiesser, "Storm surge modelling in venice: Two years of operational results," *Journal of Operational Oceanography*, vol. 9, no. sup1, s46–s57, 2016, ISSN: 1755-876X. DOI: 10.1080/1755876X.2015.1118804.

[12] L. Cavallaro, C. Iuppa, and E. Foti, "Effect of partial use of venice flood barriers," *Journal of Marine Science and Engineering*, vol. 5, no. 4, p. 58, 2017. DOI: 10.3390/jmse5040058. [Online]. Available: https://www.mdpi.com/2077-1312/5/4/58/htm.

[13] V. Fassina, M. Favaro, and D. Melica, "Brick-wall masonry decay patterns and in situ evaluation of the effectiveness of treatments of torre alberaria in venice," *Hydrophobe*, vol. 6th International Conference on Water Repellent Treatment of Building Materials, no. VI, pp. 217–234, 2011. [Online]. Available: http://hydrophobe.org/pdf/rome/vi_20.pdf.

[14] E. Vio, "La cappella di sant'isidoro e i restauri dei mosaici," *Zograf*, no. 32, pp. 117–122, 2008, ISSN: 0350-1361. DOI: 10.2298/zog0832117v.

[15] M. F. Drdácký, "Flood damage to historic buildings and structures," *Journal of Performance of Constructed Facilities*, vol. 24, no. 5, pp. 439–445, 2010, ISSN: 0887-3828. DOI: 10.1061/(ASCE)CF.1943-5509.0000065.

[16] C. Arrighi, M. Brugioni, F. Castelli, S. Franceschini, and B. Mazzanti, "Urban micro-scale flood risk estimation with parsimonious hydraulic modelling and census data," *Natural Hazards and Earth System Sciences*, vol. 13, no. 5, pp. 1375–1391, 2013, ISSN: 1561-8633. DOI: 10.5194/nhess-13-1375-2013. [Online]. Available: https://www.researchgate.net/profile/chiara_arrighi/publication/256430837_urban_micro-scale_flood_risk_estimation_with_parsimonious_hydraulic_modelling_and_census_data.

[17] D. Dassanayake, A. Burzel, and H. Oumeraci, "Evaluation of cultural losses," 2012. [Online]. Available: https://www.researchgate.net/publication/266458949_Evaluation_of_Cultural_Losses.

[18] C. Arrighi, L. Rossi, E. Trasforini, R. Rudari, L. Ferraris, M. Brugioni, S. Franceschini, and F. Castelli, "Quantification of flood risk mitigation benefits: A building-scale damage assessment through the rasor platform," *Journal of environmental management*, vol. 207, pp. 92–104, 2018. DOI: 10.1016/j.jenvman.2017.11.017.

[19] J.-J. Wang, "Flood risk maps to cultural heritage: Measures and process," *Journal of Cultural Heritage*, vol. 16, no. 2, pp. 210–220, 2015, ISSN: 12962074. DOI: 10.1016/j.culher.2014.03.002.

[20] R. Figueiredo, X. Romão, and E. Paupério, "Flood risk assessment of cultural heritage at large spatial scales: Framework and application to mainland portugal," *Journal of Cultural Heritage*, vol. 43, pp. 163–174, 2020, ISSN: 12962074. DOI: 10.1016/j.culher.2019.11.007.

[21] M. Holický and M. Sýkora, "Assessment of flooding risk to cultural heritage in historic sites," *Journal of Performance of Constructed Facilities*, vol. 24, no. 5, pp. 432–438, 2010, ISSN: 0887-3828. DOI: 10.1061/(ASCE)CF.1943-5509.0000053.

[22] A. Sardella, E. Palazzi, J. von Hardenberg, C. Del Grande, P. de Nuntiis, C. Sabbioni, and A. Bonazza, "Risk mapping for the sustainable protection of cultural heritage in extreme changing environments," *Atmosphere*, vol. 11, no. 7, p. 700, 2020. DOI: 10.3390/atmos11070700. [Online]. Available: https://www.mdpi.com/2073-4433/11/7/700/htm.

[23] H. Li, J. Zhang, J. Sun, and J. Wang, "A visual analytics approach for flood risk analysis and decision-making in cultural heritage," *Journal of Visual Languages & Computing*, vol. 41, pp. 89–99, 2017, ISSN: 1045-926X. DOI: 10.1016/j.jvlc.2017.05.001. [Online]. Available: https://www.sciencedirect.com/science/article/pii/S1045926X16301598.

[24] L. Reimann, A. T. Vafeidis, S. Brown, J. Hinkel, and R. S. J. Tol, "Mediterranean unesco world heritage at risk from coastal flooding and erosion due to sea-level rise," *Nature Communications*, vol. 9, no. 1, p. 4161, 2018, ISSN: 2041-1723. DOI: 10.1038/s41467-018-06645-9. [Online]. Available: https://www.nature.com/articles/s41467-018-06645-9.

[25] S. Fatorić and E. Seekamp, "A measurement framework to increase transparency in historic preservation decision-making under changing climate conditions," *Journal of Cultural Heritage*, vol. 30, pp. 168–179, 2018, ISSN: 12962074. DOI: 10.1016/j.culher.2017.08.006. [Online]. Available: https://www.sciencedirect.com/science/article/pii/S1296207417303527.